The Antofagasta 1995 Earthquake: Crustal Deformation Pattern as Observed by GPS and D-INSAR

Ch. Reigber, Y. Xia, G.W. Michel, J. Klotz, and D. Angermann

GeoForschungsZentrum Potsdam, Division 1: Kinematics and Dynamics of the Earth

Telegrafenberg A17, D-14473 Potsdam, Germany

reigber gfz-potsdam.de

http://www.gfz-potsdam.de

Abstract

Combinations of different ground and space techniques provide promising tools for the assessment and understanding of Geo-Hazards. We studied the spatially distributed surface deformation related to the 30 July 95, Antofagasta, Chile, subduction earthquake. In order to do this, we applied two space techniques: the Differential Interferometric SAR technique using three sets of ERS-1 SLC data and repeated GPS-measurements in a regional 70-sites' network. Results indicate that: a) co-seismic surface deformation reached values of 90 cm in the vicinity of the epicenter along the coast and values of 10 cm in a distance of 200 km to the epicenter in the direction normal to the trench; b) both the GPS-method and the D-INSAR technique provided highly comparable deformation; c) the co-seismic surface deformation field is fairly homogeneous and shows little perturbations; d) we are not yet able to distinguish between the long-term secular deformation and the earthquake event triggered deformation. Combining both methods, however, results suggest that where long-term accumulation rates of deformation are apparently high, i.e., in the western part of the investigated area, they must be homogeneously distributed.

Keywords: GPS, SAR-Interferometry, Antofagasta earthquake

Introduction

„Geo-Hazards" such as earthquakes, volcanic eruptions, and those created by land instabilities are among the strongest sudden impacts on modern life and property. Due to the increasing vulnerability of western and developing countries, future hazards appear to be increasingly disastrous with future events causing further superlatives in death and property loss. Social development in a variety of third world countries is in addition strongly hindered by recent natural hazards and the United Nations claimed the 90s as the International Decade for Natural Disaster Reduction. The assessment and mitigation of „Geo-Hazards" hence appears as an - and probably is *the* - obligatory task of the geoscience community. Hazard assessment studies are multifold and combine investigations of recurrence intervals or probability of occurrence of events together with their probable impact on life and property, and the investigation of deformation and rates within different time scales, including geological studies, paleoseismology, and the monitoring of seismicity and currently accumulating deformation. In addition to the assessment of hazards, the above mentioned studies aim at providing a better understanding of the processes acting. Studies of the regional co-seismic and post-seismic earthquake deformation embrace information about crustal and upper mantel behavior and rheologies. Within the last few years, the Global Positioning System (GPS) technology became one of the most powerful tools to derive the distribution of deformation in zones of high tectonic activity. However, measurements are conducted at discrete points and hence could miss important information between sites. A combination of the GPS-technique with the fast developing Differential Synthetic Aperture Radar Interferometry (D-INSAR) technology promises to become a major tool for the monitoring of the spatial distribution of deformation related to volcanic dome growth, mass movements or the seismic cycle (Masonnet et al., 1993, Zebker et al., 1994). This contribution presents results of the Ms:7.3 Antofagasta, Chile, of 30 July 1995 earthquake deformation study as obtained from GPS-measurements and D-INSAR.

Aims of the study are to:

investigate the 2-years' GPS-derived motions that include (pre-, co-, and post-) seismic and secular deformation and information about the amount of coupling between the Nazca and the S-American Plates;
correlate results from the GPS measurements to the D-INSAR observations;
study the co-seismic spatial distribution of surface deformation, structure-related perturbations etc.;
relate the surface deformation patterns to the along-fault quake deformation; and
(in future) investigate the post-seismic behavior of the crust and upper mantel.

The study area

The study area shown in Fig. 1 is located in N-Central Chile along the western rim of Southern America. Here, partial coupling of the subducting oceanic Nazca Plate with the upper S-American Plate causes current straining within the latter. Frequent major earthquakes occur that accommodate a large part of the ongoing deformation. Recurrence intervals of major quakes are in the order of 10s to 100s of years (Comte & Pardo, 1991; Papadimitriou, 1993). For the study area a major earthquake had been forecasted (Nishenko, 1985). Partitioning of the oblique Nazca-S-American Plate convergence has been assumed and several teleseismically derived subduction related focal plane solutions indicate almost pure thrusting.

Fig. 1: Study area

The July, 30, 1995 Ms:7.3 Antofagasta earthquake apparently ruptured 220 km of the subduction zone that starts beneath N of the Mejillones Peninsula (22.5°S) and continues to the area of Taltal to the S (25°S). The hypocentral depth was estimated between 48 km (USGS, NEIC) and 28 km (Harvard, CMT) and the corresponding fault plane indicates E-dipping thrusting apparently on the subduction interface. Second-order quake-related surface movements were not detected except for some open ruptures along the Atacama Fault, a major N-S trending system of faults that display a long history of transcurrent and normal faulting. Overall damage was relatively low.

GPS Campaign Results

Within the SAGA project (South American Geodynamic Activities) the GeoForschungsZentrum Potsdam (GFZ) established in cooperation with many partner institutions of the hosting countries in 1993/94 a network of 200 GPS stations covering the whole territory of Chile and the western part of Argentina (Klotz et al., 1996). This periodically re-observed network is embedded in a network of permanently operating stations in South America and world-wide which is primarily managed by the International GPS Geodynamics Service (IGS) (Beutler et al., 1995). The main purpose of the SAGA network is to observe station velocities over at least one decade. In combination with geologic, seismic, neotectonic, gravity and magnetic data, these velocities are used to study the ongoing deformation processes in the Andes. In the northern part of the network a dense traverse of 72 points extending from Antofagasta to the Argentine Chaco was observed 21 months before the July 1995 earthquake and 3 months after the event. Using more than 20 Trimble 4000 SSE receivers, about 3 days of continuous data were acquired on each site in each campaign. The station distribution in the subnetwork around Antofagasta is shown in Fig. 2.

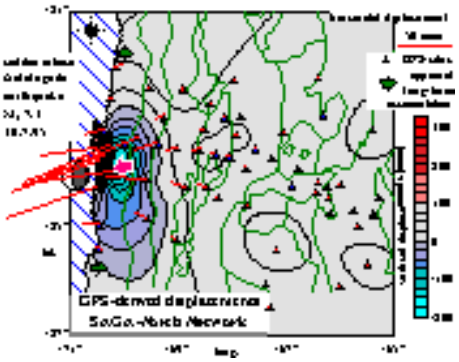

Fig. 2: SAGA-North GPS network and displacements.

The GPS data were processed with the GFZ software EPOS (Earth Parameter and Orbit Processing System). The precise GPS software package is based on undifferenced phase and pseudo-range observations. The network computation is done in form of daily solutions with the ionosphere-free linear combinations of phases and pseudoranges. In order to tie the network to the International Terrestrial Reference Frame (ITRF), the campaign data were processed simultaneously with globally distributed IGS station data and the data of permanent GFZ stations in South America. The parameters solved for are station coordinates, clock parameters, ambiguities and tropospheric parameters. Optional is the processing of orbit and Earth Orientation Parameters (EOP) in a dynamic solution. Using EPOS, different processing strategies are possible (Angermann et al., 1996). The most efficient strategy is to fix the orbits and the Earth orientation parameters to the IGS mean solution calculated by seven different centers, including GFZ Potsdam. Doing this and solving for the coordinates of all network stations and a set of global IGS sites, daily average network solutions are obtained which are referred to a system defined by the IGS orbit and EOP's. This fiducial-free network solutions were transformed to the ITRF93 using those IGS stations that were included in the global computations.

The network accuracy is assessed using the repeatability of the daily network solutions. The SAGA horizontal position accuracy depicts 1-3 mm, the vertical accuracy 5-6 mm. In the global IGS frame this network is positioned with an accuracy better than 1 cm horizontally and 1-2 cm vertically. The displacement vectors, derived from the geocentric coordinates of the two campaign solutions (see Fig. 2), are related to three sites on the stable eastern part of the South American plate: Kourou, Fortaleza and La Plata. The geometry of this station configuration is stable within 1 cm between the two measurement epochs. The displacements in the Antofagasta region are about 100 times larger than the motion in the eastern part of the network. The entire city of Antofagasta moved by about 90 cm westwards, but was only marginally moved in vertical direction. This abrupt co-seismic position change was recorded by our permanent GPS station in Antofagasta. Stations north of the epicenter were uplifted by about 30 cm, whereas the region about 100 km east of the epicenter is subsided by up to 20 cm. Figure 2 shows that an area of almost 300 x 300 km is deformed in a relatively regular form by this magnitude 7 earthquake.

Differential SAR-Interferometry Results

The study region is hyperarid with almost no vegetation. The area is hence perfectly suited for applying the differential SAR Interferometry technique (D-INSAR) for surface motion detection. The D-INSAR principle can shortly be described using the geometry of the Interferometric radar as shown in Figure 3.

Assume the surface point 0 with an orthometric height h was acquired at three different times from three different orbital positions S, S_1 and S_2 by the radar sensor. From the Interferometric pair S-S_1 with baseline B1 and the second pair S-S_2 with baseline B_2 one can obtain two interferograms with the phases F_1 and F_2, respectively, which read after removal of the Interferometric phase term of the reference surface

$$\Phi_1 = \frac{4\pi h}{\lambda r \sin\theta} B_1 \quad and \quad \Phi_2 = \frac{4\pi h}{\lambda r \sin\theta} B_2 \tag{1}$$

From these Interferometric phases the height of the surface point 0 can be determined with high resolution if the orbits are of high (5-10 cm) quality (Reigber et al., 1996). If prior to the third acquisition, point 0 was shifted by a natural or manmade event to position 0', the slant range r_2 would be changed to (r_2 - r). This change r registered by the radar sensor corresponds to the projection of the displacement vector $\overline{00'}$ onto the slant range and is independent of the baseline itself. The second phase can, therefore, be written as

$$\Phi_2' = \frac{4\pi h}{\lambda r \sin\theta} B_2 + \frac{4\pi\rho}{\lambda} \tag{2}$$

From equations (1) and (2) the change in slant range r can be derived as

$$\rho = \frac{\lambda}{4\pi}\left(\Phi_2' - \frac{B_2}{B_1}\Phi_1\right) \tag{3}$$

Before multiplying with the baseline ratio B_1/B_2, phase F_1 must be unwrapped. Under normal conditions one would also unwrap phase F_2'. But sometimes, as it was the case in our study, the baseline B_2 is too long, leading to a difficult unwrapping process of phase F_2'. In this case, the alternative procedure is to use the wrapped phase F_2' and unwrap the phase term of r.

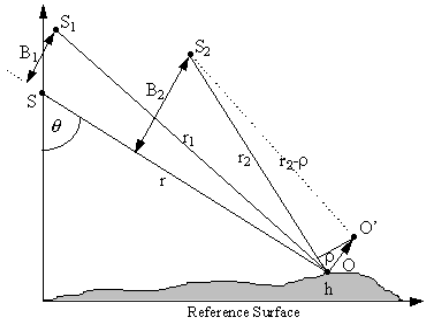

Fig. 3: Geometry of the D-INSAR.

In order to generate the D-INSAR deformation pattern from the rather complex SAR image pairs used, we followed the algorithms and procedures described in Xia (1997). A major basis for the recovery of the baselines and the reconstruction of the scene geometry is to determine the precise PRC orbits of ERS-1 using a combination of satellite laser ranging and altimeter crossover data (Massmann et al., 1994).

Unfortunately, we could find up to now only three useful ERS-1 SLC image data sets for our study area from the orbital segments

19623 - April 14, 1995; acquired before the earthquake,

21126 - July 30, 1995; acquired just a few hours after the earthquake, and

22128 - October 8, 1995; two months after the earthquake.

The location of these images is shown in Figure 1.

The repetition frequency (PRF) was different for the three data takes. Therefore, data sets 21126 and 22128 were first resampled and then registered with PRF 1679.90 Hz of data set 19623. The calculated baselines and fringe frequencies are given in Figure 4. The total image size is 140 km in along-track direction and 40 km cross track.

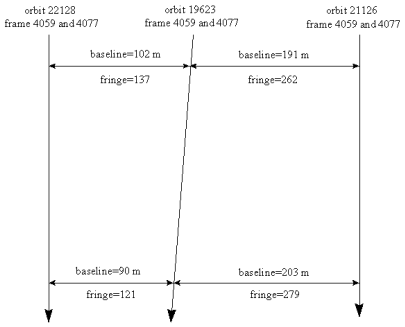

Fig. 4: Distribution of the baselines and fringes.

Because the baseline of image pair 19623/22128 is better suited for phase unwrapping, this pair was chosen for generating the reference topography. The images 19623/21126 were taken as second pair. Due to the timely distribution of the images, it is evident that in our case both data pairs are affected by earthquake-induced dislocation and that equation (1) therefore has to be modified in the same way as equation (2). This leads to the modified equation (3).

$$\left(1-\frac{B_2}{B_1}\right)\rho=\frac{\lambda}{4\pi}\left(\frac{B_2}{B_1}\Phi_1-\Phi_2\right) \tag{4}$$

The (1 - B_2/B_1) scaling factor of the change r is in our case approximately 3 (B_1 = -96 m, B_2 = 197 m). Thus the phase difference of 2p in the differential interferogram will correspond to a displacement of 0.9 cm in slant range direction.

Fig. 6 displays the radar intensity and the Interferometric fringe images. Fig. 7 shows the coherence image, the differential interferogram with the topography removed and representing the deformation in slant range direction, and the topography derived from data pair 19623/21126 from which the displacement term was removed. A few facts become immediately evident from these pictures. The dark stripes in the coherence image indicate unstable operation of the SAR sensor (orbit 22128, frame 4059). The orientation of the Interferometric fringes is considerably perturbed by the crustal deformation. The differential interferogram clearly shows that the deformation increases from the top to the bottom of the image.

Comparison of D-INSAR and GPS-derived deformation

From its spatial resolution D-INSAR is a one-dimensional observation technique whereas GPS provides three-dimensional position information. To compare results from both techniques we projected the GPS-derived 3D-displacement vectors into slant range direction using the precise orbital positions of ERS-1 as computed by the D-PAF. Figure 5 shows two „deformation in slant range" surfaces, one from D-INSAR and one derived using the interpolated GPS data. They coincide largely. Five GPS points 0, 3, 4, 34 and 2014 are located in the processed D-INSAR deformation image (Fig. 7). Direct comparison of results from both techniques is hence possible for these sites. In order to further test the D-INSAR results we extrapolated the resolving deformation patterns beyond the lower bound of the image, i.e., to the south where the GPS stations 1 and 6 are located. Table 1 includes a comparison of results for these seven points.

Station m	GPS absolute	GPS relative	D-INSAR relative	Difference
0	-25.09	0	0	0
3	-5.32	197.7	189	8.7
4	-27.25	-21.6	-18	-3.6
2014	-19.56	55.3	54	1.3
1	6.43	315.2	about 300	15.2
6	-25.27	-1.8	about -1	-0.8
34	3.86	289.5	282	7.5

Table 1: Comparison of displacement results from GPS and D-INSAR (all in slant range direction in mm).

The average difference for the directly comparable points 0, 3, 4, 2014 and 34 is 5 mm and for the extrapolated points less than 20 mm.

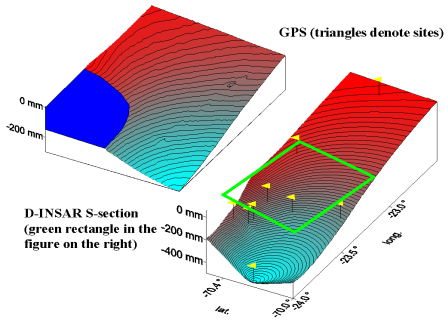

Fig. 5: Comparison of D-INSAR and GPS derived deformation in slant-range direction.

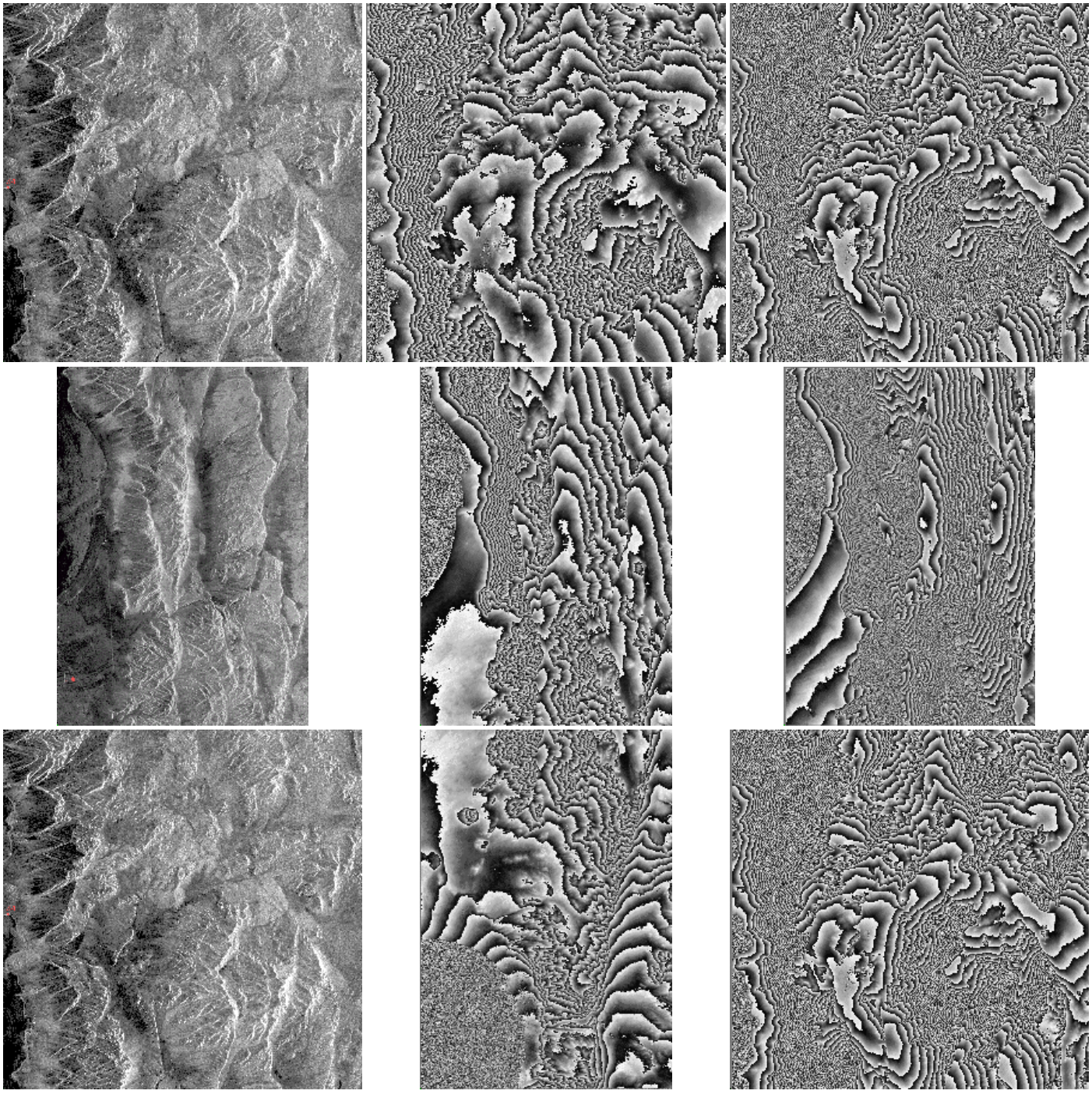

intensity *fringe, 19623/22128, baseline 96 m* *fringe , 19623/21126, baseline 197 m*

Fig. 6: intensity and fringe images

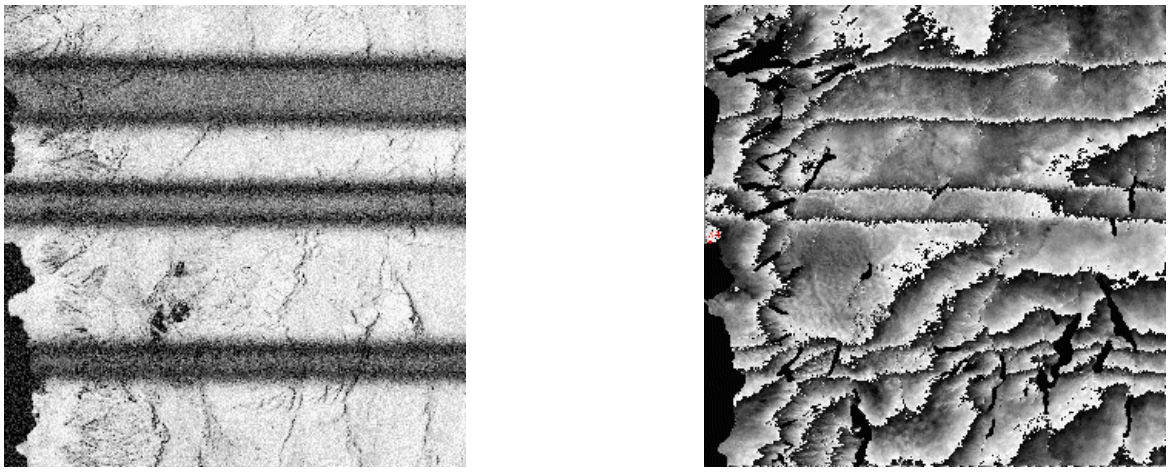

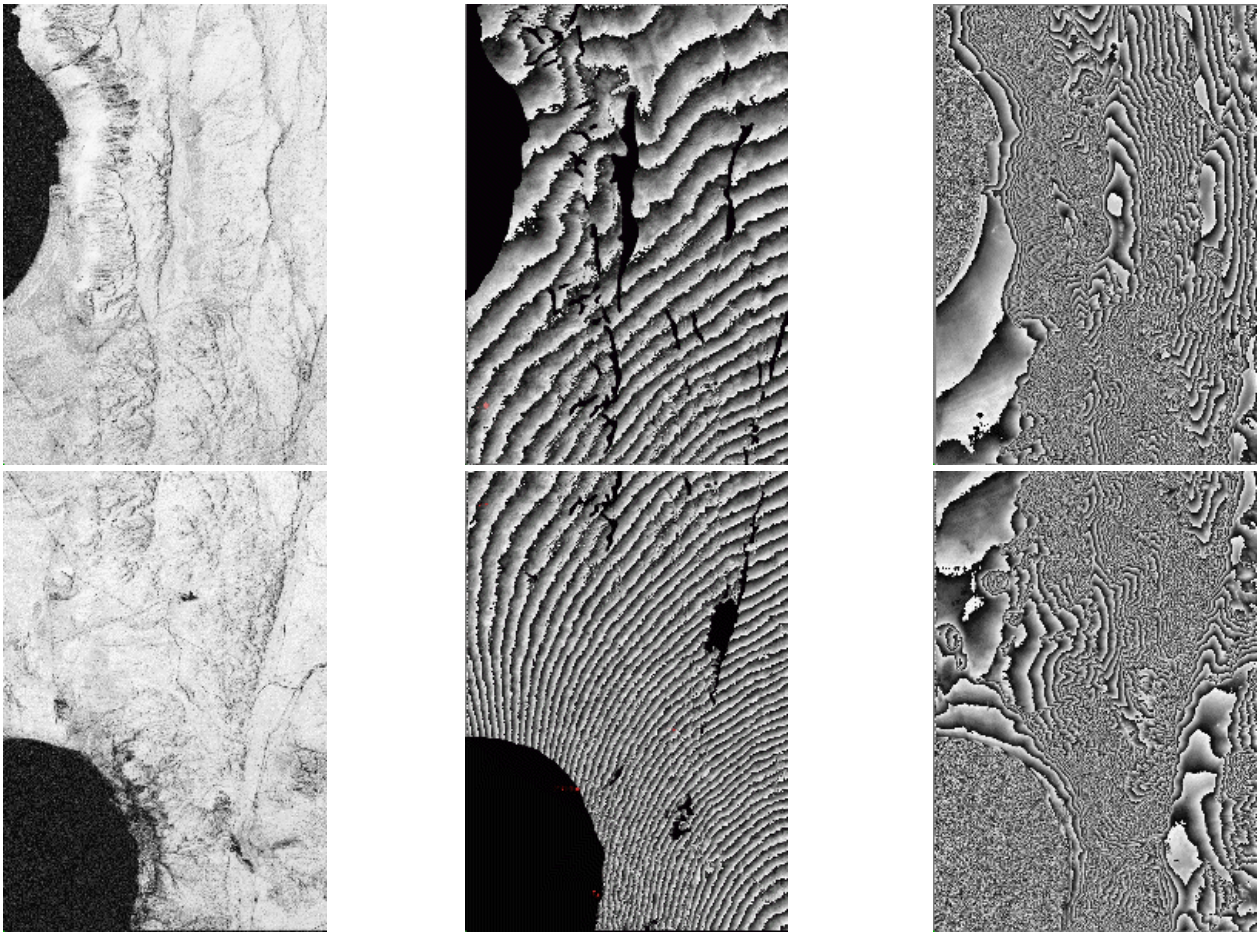

coherence (19623/22128)

deformation (0.9 cm per fringe) derived from 19623/22128 and 19623/21126

topography (50 m contour) derived from 19623/21126 and differential interferogram

Fig. 7: coherence, deformation and topography images

The deformation patterns derived using both techniques coincide, suggesting that a major part of the resulting deformation happened between April 14 and July 30 and hence is co-seismic. However, we cannot exclude that a minor part of the deformation is not related to the event but indicates pre-seismic or inter-seismic straining or a-seismic deformation. We suggest that the eastward directed movements detected at the northernmost and southernmost GPS stations (Fig. 2) indicate apparent inter-seismic accumulation of deformation prior to the earthquake event. Further studies are necessary to distinguish long-term straining from short-term event-induced deformation.

Only minor perturbations were found in the D-INSAR fringes. In addition, deformation patterns interpolated using the GPS-derived motions suggest that the major part of the deformation was fairly homogeneous. Second-order movements along crustal faults triggered by the major quake are therefore not depicted by the data. Minor perturbations, which are evident in the fringe patterns, correlate with marked changes in topography and changes in lithologies. This is especially true a) adjacent to the coast where soft coastal sediments border crystalline Jurassic volcanic rocks and b) locally within neotectonic fault zones where fine cataclastic material facilitate quake-induced sediment redeposition.

Conclusions

A combination of D-INSAR and GPS techniques was used to depict co-seismic deformation triggered by the Ms: 7.3 1995 Antofagasta, Chile, subduction earthquake. The 72-sites' GPS network covers an area of over 300 km normal to the Chilean trench. Results indicate significant co-seismic deformation over at least 200 km off the epicenter and normal to the trench. The D-INSAR data cover only a limited area - near the coast and adjacent to Antofagasta - where 7 GPS sites are located. Deformation patterns derived using both techniques coincide and show only minor differences. This suggests that a) the major part of the 2-years GPS-monitored deformation was co-seismic and b) co-seismic deformation was distribute almost homogeneously. The latter is backed up by the fact that movements along second-order crustal faults, which might have been triggered by the major quake, were not detected. We are not yet able to distinguish between long-term accumulation of deformation and event-triggered release. Applying both techniques, their high accuracy and low relative differences in motion encourage us, however, to use these techniques further-on to quasi-monitor the expected elastic inter-seismic accumulation of deformation as well as the post-seismic visco-elastic deformation expected. The latter embraces information on the rheology of the crust and upper mantle and about the long-term emergence of the Coastal Cordillera. Monitoring future deformation will be especially interesting in the north of the study area where an earthquake has long been expected. In spite of the high earthquake magnitude, damage was low in the area of Antofagasta. This can be explained partly by the behavior of the underground. We think that the high-resolution D-INSAR deformation data entangle further information on the quake-induced behavior of the underground and soil and may thus - together with GPS -in future directly assist hazard assessment studies.

Altogether, the results obtained so far are encouraging for various modeling groups within GFZ and motivated us to start operation of the 4 m mobile ground station recently purchased by DLR and GFZ. First measurements were conducted in Cordoba/Argentina in January 1997. ERS-1 SAR data have already been processed and will be integrated into our studies of the post-earthquake surface deformation processes. In addition, we will soon install a few corner reflectors in the study area to increase the recovery accuracy of the image geometry and the GPS station identification in the images (<1 pixel).

References

Angermann, D., G. Baustert, J. Klotz, J. Reinking, S.Y. Zhu, 1996
Hochgenaue Koordinatenbestimmung in großräumigen GPS-Netzen. *Allgemeine Vermessungs-Nachrichten*, Heft 5, H. Wichmann Verlag.

Beutler, G., I.I. Mueller & R. Neilan, 1996
The International GPS Service for Geodynamis (IGS): The Story, *Proc. IAG Symposium,* No 115, Springer Verlag, ISBN 3-540-60872-6.

Compte, D. & M. Pardo, 1991
Reappraisal of great historical earthquakes in the Northern Chile and Southern Peru seismic gaps. *Natural Hazards*, **4**, 23-44.

Klotz, J., J. Reinking & D. Angermann, 1996
Die Vermessung der Deformation der Erdoberfläche, *Geowissenschaften*, **14**, 389-394.

Masonnet, D., M. Rossi, C. Carmona, F. Adregna, G. Peltzer, K. Feigl & T. Rabaute, 1993
The displacement field of the Landers earthquake mapped by radar interferometry, *Nature*, **364**, 138-142.

Massmann, F.-H., Ch. Reigber, R. König, J.C. Ralmondo & C. Rajasenan, *1993*
ERS-1 orbit information provided by D-PAF. *Proceedings Second ERS-1 Symposium - Space at the Service of our Environment, Hamburg, Germany, 11-14 October 1993, ESA SP, **361**, 765-770.*

Nishenko, S.P., 1985
Seismic potential for large and great intraplate earthquakes along the Chilean and southern Peruvian margins of South America: A quantitative reappraisal . *J. Geophys. Res.*, **90**, 3589-3615.

Papadimitriou, E.E., 1993
Long-term earthquake prediction along the western coast of South and Central America based on a time predictable model, *PAGEOPH*, **10**, 301-316.

Reigber, Ch., Y. Xia, H. Kaufmann, F.-H. Massmann, L. Timmen, J. Bodechtel & M. Frei, 1996
Impact of the Precise Orbit on the SAR-Interferometry, *Proc. ESA Workshop on the Applications of the ERS SAR Interferometry*, Zürich.

Xia, Y., 1997
Processing of SAR data from the mobile DLR/GFZ antenna, *GFZ Scientific Technical Report*, in preparation.

Zebker, H., P.A. Rosen, R.M. Goldstein, A. Gabriel & Ch. Werner, 1994
On the derivation of coseismic displacement fields using differential radar interferometry: The Landers earthquake, *J. Geophys. Res.*, **99**, 19617-19634.